

WegCenter/UniGraz Technical Report for ESA/ESTEC No. 2/2006

Project:

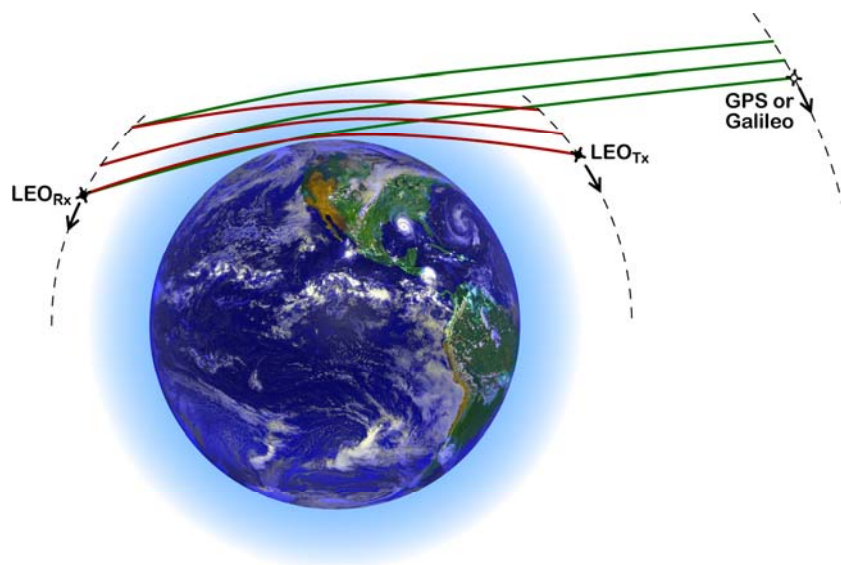
Prodex-CN1 – Advanced Topics in RO Modelling and Retrieval
[ESA Prodex Arrangement No. 90152-CN1]

Advanced Retrieval Processing Chain for Derivation of Atmospheric Profiles from LEO-LEO Radio Occultation Data

G. Kirchengast¹, S. Schweitzer¹, M. Schwaerz¹, J. Fritzer¹, and M. Gorbunov^{2,1}

¹Wegener Center for Climate and Global Change (WegCenter), University of Graz, Graz, Austria

²Institute of Atmospheric Physics (IAP), Russian Academy of Sciences, Moscow, Russia



July 2006

(intentionally left blank; back page if double-sided print)

Table of Contents

1. INTRODUCTION	1
2. THE EGOPS5 SOFTWARE	3
2.1. EGOPS5 Overview.....	3
2.2. Overview on the Retrieval Processing Chain for LEO-LEO Data	4
3. DESCRIPTION OF PROCESSING CHAIN AND RETRIEVAL ALGORITHMS....	9
3.1. Bending Angle Retrieval	9
3.2. Transmission Retrieval.....	15
3.3. Real Refractivity Retrieval	17
3.4. Imaginary Refractivity/Absorption Coefficient Retrieval	18
3.5. Atmospheric Profiles Retrieval.....	19
4. SUMMARY AND CONCLUSIONS.....	24
REFERENCES	25

(intentionally left blank; back page if double-sided print)

List of Acronyms

ACCURATE	Atmospheric Climate and Chemistry in the UTLS Region and Climate Trends Explorer
ACE+	Atmosphere and Climate Explorer mission (ESA mission concept 2002–2004)
ACEPASS	ACE+ Phase A Scientific Support Study (ESA study 2002-2004)
BLUE	Best Linear Unbiased Estimation (or Estimator)
CIRA86aQ	Enhanced (moist air) version of the classical COSPAR International Reference Atmosphere (CIRA) model (empirical atm. model; Kirchengast et al., 1999)
COSPAR	Committee on Space Research (international scientific organization)
E5L	EGOPSS5 LEO-LEO (processing)
ECEF	Earth Centered Earth Fixed (coordinate system)
ECMWF	European Centre for Medium-Range Weather Forecasts (Reading, U.K.)
EGOPSS5	End-to-end Generic Occultation Performance Simulator, Version 5
ESA	European Space Agency
ESA-Prodex	An ESA Programme line (for an enlisted subgroup of member states, incl. Austria)
ESTEC	European Space research and Technology Centre (of ESA)
FIR	Finite Impulse Response (filter)
FoMod	Forward Modeling System, subsystem of EGOPS
Galileo	European future global navigation satellite system
GNSS	Global Navigation Satellite Systems (Global Positioning System GPS, and Galileo)
GO	Geometric optics
GPS	Global Positioning System
GRO	GNSS-LEO Radio Occultation (here Galileo & GPS L band signals, ~1.2 / 1.6 GHz)
InRet	Inversion/Retrieval, subsystem of EGOPS
IR	Infrared spectral region
LEO	Low Earth Orbit
LIO	LEO-LEO Infrared Occultation (here laser cross-link signals within 2–2.5 μm)
LRO	LEO-LEO Radio Occultation (here MW cross-link signals within 3–30 GHz)
MAnPl	Mission Analysis Planning System, subsystem of EGOPS
MSIS90	Mass Spectrometer Incoherent Scatter model 90 (empirical atm. model; Hedin, 1991)
MW	Microwave spectral region
OPAC	Occultations for Probing Atmosphere and Climate
OSMod	Observation System Modeling, subsystem of EGOPS
POD	Precise Orbit Determination
Prodex-CN1	“Prodex-Change Notice 1” project; continuation project of previous Prodex project
RO	Radio Occultation
Rx	Receiver (satellite)
SNR	Signal-to-Noise Ratio
Tx	Transmitter (satellite)
UniGraz	University of Graz (Austria)
UTLS	Upper Troposphere/Lower Stratosphere height region
WegCenter	Wegener Center for Climate and Global Change (at UniGraz)
WO	Wave optics
X/K band	Microwave band covering the frequencies 7–40 GHz

(intentionally left blank; back page if double-sided print)

1. Introduction

This report deals with Task 1.3 of the Prodex-CN1 Project “Advanced Topics in Radio Occultation Modelling and Retrieval” of ESA, which was concerned with advanced atmospheric profiles retrieval from LEO-LEO radio occultation (LRO) data. The LRO retrieval chain proceeds from bending angle and transmission, via real and imaginary refractivities to temperature and humidity, including capability of differential transmission retrieval.

The Task 1.3 work was in particular concerned with upgrading the EGOPS5 (End-to-end Generic Occultation Performance Simulator, Version 5) software with a retrieval chain also capable of differential transmission retrieval and other related improvements such as in noise filtering and improved integration of LRO retrieval algorithms with GNSS-LEO radio occultation (GRO) algorithms.

The report is structured as follows. After a brief overview on the EGOPS5 software, and in particular on the structure and elements of the LRO retrieval processing chain, in section 2, the report provides a detailed description of the processing chain and retrieval algorithms at the status after the advancements by the Prodex-CN1 Project in section 3.

The bending angle and transmission retrieval part is in this context described for the geometric-optics data processing approach. Thus, as a complementary report to this one from Tasks 1.1 and 1.2 of the Prodex-CN1 Project, the companion report by Gorbunov et al. (2006) provides a detailed description of the wave-optics based bending angle and transmission retrieval. We note that a relevant less detailed baseline description was given by Gorbunov and Kirchengast (2005a) within the context of the previous ESA project ACEPASS.

The report will be of significant utility also beyond the algorithmic documentation of the specific EGOPS5 LRO processing chain, since it is the so far most detailed description of LRO retrieval algorithms also in a generic sense. It thus provides valuable information for anyone interested to learn about LRO processing in more depth than covered by other sources.

(intentionally left blank; back page if double-sided print)

2. The EGOPS5 Software

2.1. EGOPS5 Overview

The End-to-end Generic Occultation Performance Simulator/Version 5 (EGOPS5) is a software package allowing the end-to-end simulation of GRO and LRO measurements. Its main purpose is to support research addressing scientific and mission analysis questions on the GNSS-LEO/LEO-LEO based radio occultation technique. It is composed of a series of modules which are integrated into so-called Systems (see Figure 1 below).

The Mission Analysis and Planning (MANPI) System allows analysis and planning of GNSS-LEO and LEO-LEO satellite constellations with regard to their suitability for occultation missions. In particular, its main capability is that the distribution of occultation events around the globe can be simulated using arbitrary (user-generated) satellite constellations.

Based on the resulting geometry data of such occultation events, the Forward Modeling (FoMod) System together with the Observation System Modeling (OSMod) System enables quasi-realistic simulation of GRO as well as LRO radio occultation observables (i.e., phase and amplitude profiles at each signal frequency) and related required variables. In particular, FoMod's task is to simulate the electromagnetic signal propagation through the atmosphere (and ionosphere) towards the receiver based on orbital motions of transmitter and receiver satellites. The resulting occultation signals are influenced by atmospheric (and ionospheric) effects. Effects due to the receiving system (instrumental errors, in general), which usually perturb the signal quality, are superimposed during the subsequent OSMod simulation.

Finally, the Inversion/Retrieval (InRet) System is responsible for the retrieval processing of simulated or observed GRO/LRO phase and amplitude data (supplemented by the necessary geometry information) in order to obtain quasi-vertical profiles of atmospheric parameters. The retrieval algorithms for GRO and LRO differ somewhat: In the case of LRO, phase and amplitude data are converted via bending angles and transmissions down to profiles of refractivity and absorption coefficients, density, pressure (or geopotential height), temperature, and humidity (as well as liquid water if needed). In the case of GRO, only bending angles are exploited, which is why no (frequency-dependent absorption coefficients can be utilized to independently retrieve humidity. A description to some mid-level detail of the scientific retrieval algorithms for both GRO and LRO data processing was given by Kirchengast et al. (2004a). The present report now provides an in-depth description of the processing chain and retrieval algorithms for LRO geometric-optics data processing at the status after the advancements by the Prodex-CN1 Project. Wave-optics bending angle and transmission retrieval is described by the companion reports of Gorbunov et al. (2006) and Gorbunov and Kirchengast (2005a) as noted in section 1.

The four systems briefly introduced above are the core of EGOPS5. Additionally, as Figure 1 illustrates, there are input interfaces for the four systems (left column block in Figure 1) and there is a so-called Visualization/Validation System (bottom block of Figure 1), which enables post-processing of the retrieved data (statistics, etc.) as well as visualization, including the capability to extract information from the atmosphere system underlying the occultation simulations. Altogether, EGOPS5 with its comprehensive end-to-end simulation capabilities enables research contributing to a better quantification of the potential of the GRO and LRO techniques for atmosphere and climate science.

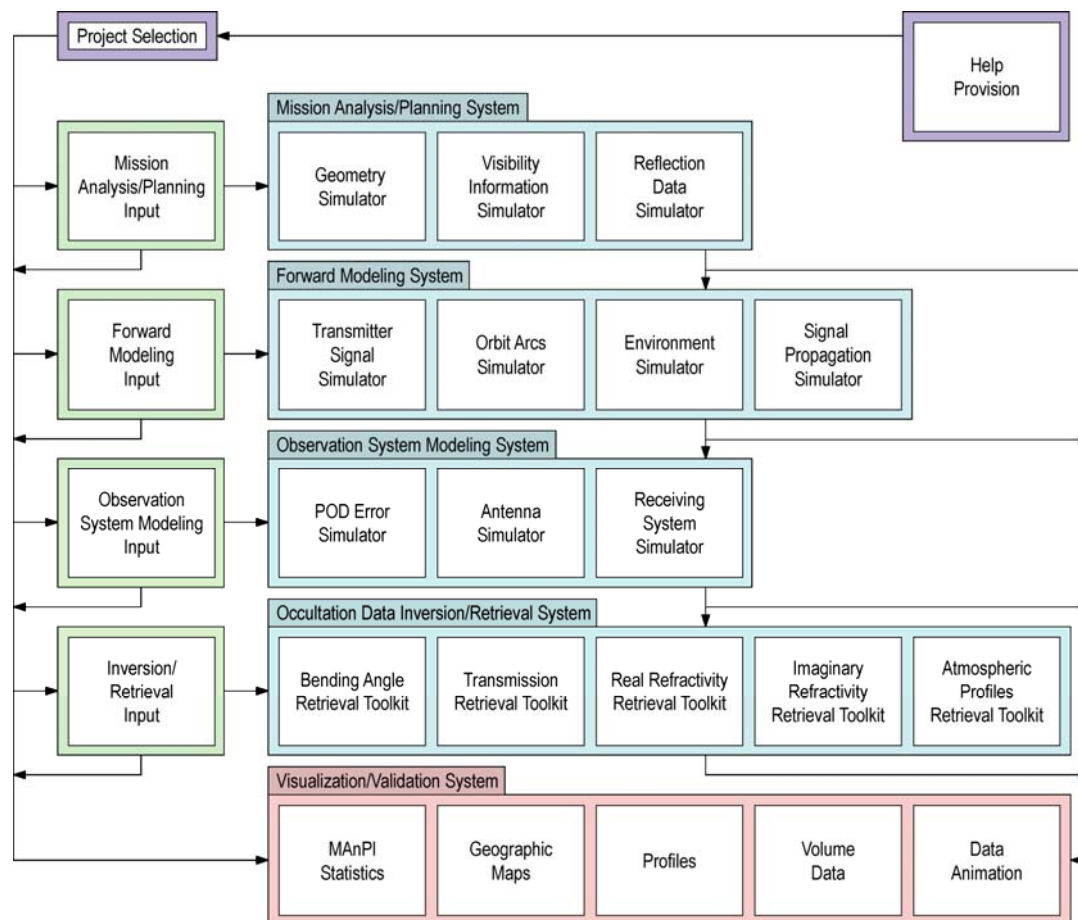


Figure 1: Modular view of EGOPS5 (after Kirchengast et al., 2004b).

2.2. Overview on the Retrieval Processing Chain for LEO-LEO Data

Inversion/Retrieval of LEO-LEO occultation data denotes the processing of simulated or observed phase and amplitude data, supplemented by the necessary geometrical information, via Doppler shifts, bending angles and transmissions down to quasi-vertical atmospheric profiles of real and imaginary refractivities, density, pressure (or geopotential height), temperature, humidity, and liquid water.

The retrieval processing strategy for LEO-LEO measurements within EGOPS5 consists of the following five main steps:

- bending angle retrieval,
- transmission retrieval,
- real refractivity retrieval,
- imaginary refractivity/absorption coefficient retrieval, and
- atmospheric profiles retrieval.

The general processing concept is illustrated in Figure 2, and the related general procedure is as follows. A detailed description on each of the five steps is given in section 3 below.

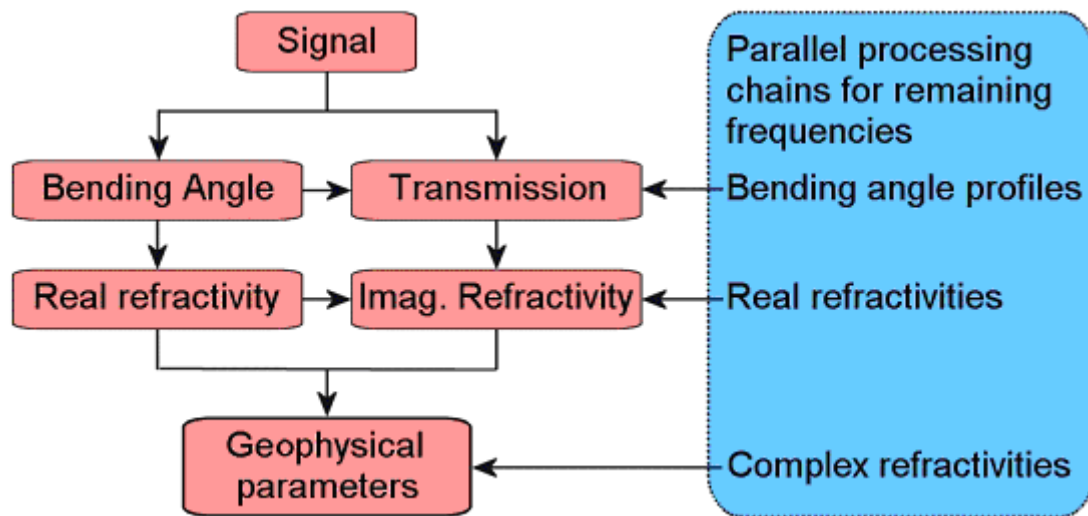


Figure 2: LEO-LEO retrieval processing chain overview. The five upper boxes to the left represent the processing chain for a single frequency channel, whereas the box to the right represents parallel processing chains for the remaining carrier frequencies in the system. (after Nielsen et al., 2005).

First, the phase and amplitude profiles (“Signal”) are used together with the corresponding precise orbit determination (POD) data comprising positions and velocities of LEO transmitter and LEO receiver satellites to determine the atmospheric bending angle profile as a function of impact parameter in the same way as this is performed in the well-known GNSS-LEO processing (e.g., Nielsen et al. 2005). If wave-optics processing is utilized, both phase path changes (Doppler shift profiles) and normalized amplitude profiles (raw transmission profiles) are used in this process, if only geometric-optics processing is performed only Doppler shift profiles are used. For details on this first step see section 3, subsection 3.1.

Second, the amplitude profiles at each LEO-LEO signal frequency (e.g., the LRO frequencies of the ACE+ mission concept have been 9.7 GHz, 17.25 GHz, 22.6 GHz; see, e.g., Kirchengast et al., 2004a), the impact parameter profile, and the POD transmitter and receiver position profiles are used to compute the transmission profiles due to atmospheric absorption at each frequency. Differencing of log-transmission profiles of two frequencies leads to differential transmission profiles, which can be used alternatively to direct transmission in subsequent processing steps. The exact way of how amplitude defocusing and spreading is subtracted from the measured amplitude profiles, in order to obtain the transmission profiles due to absorption only, depends on whether wave-optics or geometric-optics processing is utilized. For details on this second step see section 3, subsection 3.2.

Third, the bending angle profile as a function of impact parameter is converted to the real refractivity profile as a function of height via the classical Abel transform well-known from GNSS-LEO processing. For details on this third step see section 3, subsection 3.3.

Fourth, the real refractivity profile and the impact parameter profile are used together with the (differential) transmission profiles at each LEO-LEO frequency to derive the (differential)

imaginary refractivity profile as a function of height of each frequency (pair) with another Abel transform akin to the classical one. This transform has the same Abelian integration kernel but is different in its integrand. Since (differential) imaginary refractivity is proportional to the (differential) absorption coefficient, the latter can be obtained alternatively or in addition. For details on this fourth step see section 3, subsection 3.4.

Fifth, the real refractivity profile and the (differential) imaginary refractivity profiles of each LEO-LEO frequency (pair), all as functions of height, are used, together with the equations relating temperature, humidity, pressure, and cloud liquid water (“geophysical parameters”) to real and (differential) imaginary refractivity, in order to derive the atmospheric profiles of the geophysical parameters as function of height. In addition, the geopotential height of pressure levels can be obtained from the knowledge of pressure as a function of (geometric) height. The key equations involved are the real refractivity equation (“Smith-Weintraub formula”), the hydrostatic equation, the equation of state, and the spectroscopic equations for computing the frequency-dependent absorption coefficient from the geophysical parameters (e.g., “Liebe Model”). Figure 3 below provides a schematic overview on this LEO-LEO atmospheric profiles retrieval chain.

As Figure 3 (bottom part) shows, this geophysical parameter estimation problem is efficiently solved by downward (in height) integration of the hydrostatic equation combined with an iterative BLUE (best linear unbiased estimation) solution at each integration step for obtaining at the given height level temperature, humidity, and liquid water from the real and imaginary refractivity values. The BLUE algorithm requires the specification of covariance matrices for the (differential) refractivity data, which are formulated based on the knowledge of their respective error characteristics.

If the (differential) imaginary refractivity variances grow large into the lower troposphere (e.g., under conditions of significant atmospheric turbulence), so as to render the BLUE problem effectively under-determined, it is advisable to include also adequate prior temperature values plus their variance into the estimator to ensure accurate geophysical parameter estimation also under these conditions. With new wave-optics based bending angle and transmission retrieval algorithms (Gorbunov and Kirchengast 2005a,b; 2006) such inclusion of prior temperature information will be rarely required, however. For details on this fifth step see section 3, subsection 3.5.

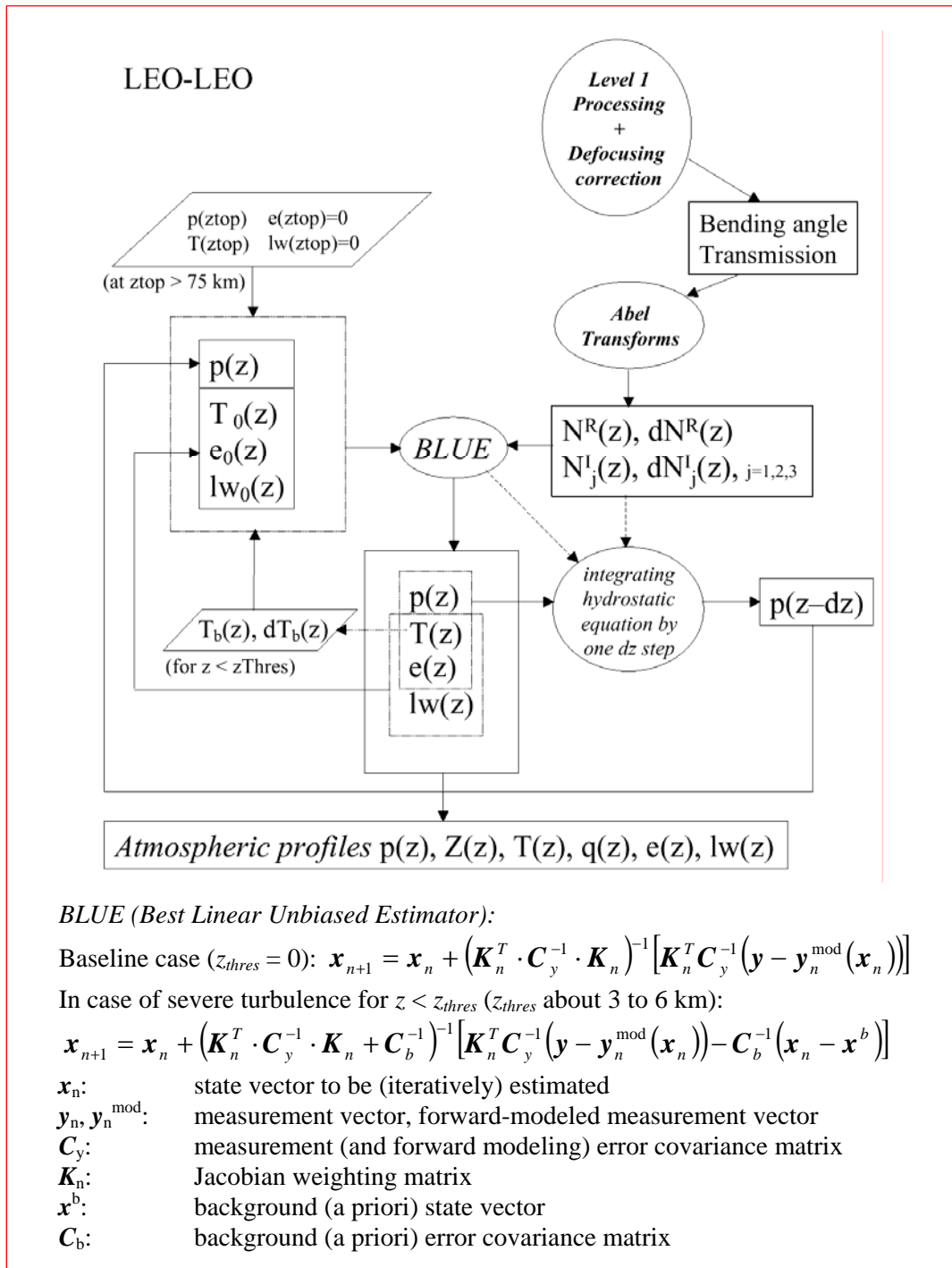


Figure 3: Schematic view of the LEO-LEO atmospheric profiles retrieval algorithm in EGOPS5 together with a summary on the BLUE process (from Kirchengast et al., 2004a). The input chain to the atmospheric profiles retrieval, connecting via the Abel Transforms, is also indicated.

(intentionally left blank; back page if double-sided print)

3. Description of Processing Chain and Retrieval Algorithms

3.1. Bending Angle Retrieval

The derivation of bending angle profiles as function of the impact parameter can be performed either via a geometric-optics (GO) or a wave-optics (WO) approach. In the EGOPS5 LEO-LEO processing both approaches are implemented of which the GO processing for bending angle retrieval is described here. On the WO processing approach for bending angle retrieval see Gorbunov et al. (2006), Nielsen et al. (2005), and references therein.

LEO-LEO GO bending angle retrieval uses as input observables the measured phase profiles at the LEO-LEO signal frequencies and the transmitter and receiver orbital positions and velocities from POD, and proceeds in five steps:

- smoothing (and outlier rejection)
- ionospheric correction of phases
- derivation of Doppler shift from the corrected phase delay
- derivation of bending angle and impact parameter from the Doppler shift
- statistical optimization of bending angles at high altitudes

The LEO-LEO bending angle retrieval is in general identical to the GNSS-LEO one. Extensive literature thus exists describing it in different variants, all, if properly implemented, leading to the same results. Useful general descriptions include Melbourne et al. (1994), Kursinski et al. (1997), Steiner (1998), Syndergaard (1999), Kursinski et al. (2000) and Nielsen et al. (2005), but there are many others. Below the equations for each of the five steps are summarized with focus on their specific implementation in EGOPS5 LEO-LEO (E5L) processing.

Smoothing (and outlier rejection).

Data smoothing over ~1 sec (~2 km in height, less below 30 km) is commonly applied to simulated or measured phase path delays at sampling rates of 10 Hz (~0.2 km in height) or higher before ionospheric correction and Doppler shift derivation. This avoids unnecessary amplification of high-frequency noise. Given the countless number of digital filter possibilities, many smoothing variants are possible, the most simple one being a standard “moving average” FIR filter.

In E5L processing, a regularization smoother of the form

$$\tilde{\varphi} = (\mathbf{I} + \lambda \mathbf{S}^T \mathbf{S})^{-1} \cdot \varphi \quad (1)$$

$$\lambda = 10^{\frac{f_s [\text{Hz}]}{10}} \quad (2)$$

φ ... measured phase delay vector $\{\varphi_j(t_i)\}$; occultation rays $i = 1, \dots, N$; signal frequencies j (baseline from ACE+: $j = 1, \dots, 3$)

$\tilde{\varphi}$... smoothed phase delay vector $\{\tilde{\varphi}_j(t_i)\}$

\mathbf{S} ... N×N smoothing matrix (third difference operator)

\mathbf{I} ... N×N unit matrix

λ ... regularization parameter

f_s ... sampling rate (for GO processing $f_s = 10$ Hz)

is applied to the raw $\varphi_j(t_i)$ profiles, following Syndergaard (1999), section 3.1.1 therein. A 3rd-order difference operator is used for the smoothing matrix \mathbf{S} , and $\lambda = 10$ for the GO processing sampling rate of 10 Hz. This filtering yields a vertical resolution of ~ 2 km above 30 km, increasing to < 1 km in the troposphere. The result in general is not very different from other filters with similar transfer function but compared to, e.g., standard “moving average” FIR filters, it is more robust against intermittent noise “spikes” in the data.

For simulated phase delay data with orderly simulated random error sources, genuine outliers (un-physical data values) do not occur. Thus currently the E5L processing has outlier rejection for $\varphi_j(t_i)$ not activated. However, a “3- σ rejection” algorithm, curing for data samples deviating by more than 3 standard deviations from the mean over a neighborhood of ± 0.5 sec, is prepared for activation as required.

Ionospheric correction of phases.

The simple linear dual-frequency combination of the form

$$\varphi(t_i) = \frac{f_1^2}{f_1^2 - f_2^2} \cdot \tilde{\varphi}_1(t_i) - \frac{f_2^2}{f_1^2 - f_2^2} \cdot \tilde{\varphi}_2(t_i) \quad (3)$$

t_i ... occultation event time, time of data sample i ; $i = 1, \dots, N$

f_1, f_2 ... LEO-LEO signal frequencies (baseline from ACE+: $f_1 = 9.7$ GHz, $f_2 = 17.25$ GHz, $f_3 = 22.6$ GHz)

$\tilde{\varphi}_1, \tilde{\varphi}_2$... smoothed phase delay at frequency f_1, f_2

φ ... atmospheric phase delay

is used to eliminate the ionospheric phase delay from the measured total phase delays, $\tilde{\varphi}_{1,2}(t)$, in order to obtain the (neutral) atmospheric phase delay $\varphi(t)$. The physical basis is the inverse-squared frequency dependence of ionospheric refractivity (e.g., Budden, 1985). Eq. (3) is sequentially applied to each individual data sample in the profile.

For frequencies near 10 GHz and higher, the ionospheric effects are about 2 orders of magnitude smaller than in the GNSS-LEO L-band case so more sophisticated correction schemes than Eq. (3), such as the correction of bending angles commonly used for GNSS-LEO (Vorob'ev and Krasnil'nikova, 1994), are not required. In addition, the SNR at altitudes above 30 km is much higher than in the GNSS-LEO case so that the accuracy of LEO-LEO bending angles can be expected to be significantly better in the upper stratosphere and mesosphere, potentially limited by residual clock and POD errors rather than residual ionospheric errors and thermal noise as for GNSS-LEO (Ramsauer and Kirchengast, 2001). High-quality clocks (USOs) are thus the key for realizing the much superior stratospheric performance potential of LEO-LEO phase data over GNSS-LEO as far as possible.

In E5L processing, currently the lowest two frequencies (e.g., in case of ACE+ the frequencies $f_1 = 9.7$ GHz and $f_2 = 17.25$ GHz) are used for the correction, and the resulting $\varphi(t)$ is assigned to f_1 . More sophisticated utilization of all pairs of f_1, f_2 , and f_3 is possible for fur-

ther incrementally improved correction but not really found warranted for frequencies at 10 GHz and beyond, where ionospheric influence have become very small. Perhaps more important practically is that additional frequencies may provide useful redundant information for intrinsic quality control and verification.

Derivation of Doppler shift from the corrected phases.

Doppler shift is derived from phase delay $\varphi(t_i)$ via differentiation

$$d(t_i)[m/sec] = \frac{d\varphi(t_i)}{dt}, \quad d_j(t_i)[Hz] = -\frac{f_j}{c} d(t_i) \quad (4)$$

$d(t_i)$... Doppler shift profile

f_j ... LEO-LEO signal frequency

c ... velocity of light (in vacuum) ($c = 299792458$ m/s)

and is the key observable for determining the bending angle to which it is closely proportional via the sinking/rising velocity of ray paths during an occultation event (e.g., Rieder and Kirchengast, 2001a). Eq. (4) shows that absolute phase delay need not be known as the Doppler shift retains only the phase change, which is the observable to be accurately tracked over the duration of ~1 min during an event.

This accurate tracking is ensured by the high short-term stability (over 1–100 sec) of on-board USO frequency standards. Exactly here is the heart of the often quoted intrinsic self-calibration of refractive occultation data: each single Doppler shift profile in itself, together with its associated precise orbital position and velocity profiles from POD, is an absolute measure of height-dependent atmospheric bending angle at the time and geographic location of the event, independent of any reference or calibration data, independent of any other real or potential measurements before, in parallel, or after the 1-min event. This is also the basis, which justifies notions like “unique climate benchmark measurements” or “unique long-term stability over decades from unique short-term stability over seconds”. It is, in particular, justified if the on-board USO frequency standard is systematically traced back to the international time standard (“SI traceability”; e.g., Leroy et al., 2006). Ensuring such traceability is possible by careful implementation of USO time transfer, for example, via GPS time to UTC.

In E5L processing, the phase differentiation in Eq. (4) is implemented as a space-centered finite difference, i.e., the Doppler shift of each sample is set to the difference estimate between the neighbor samples above and below (with due care at the profile boundaries). This simple scheme is possible since the regularization smoother, Eq. (1), strictly ensures smoothness of the data over each neighborhood of 3 data samples.

Derivation of bending angle and impact parameter from the Doppler shift.

The conversion equations from Doppler shift $d(t)$ and orbital positions $\mathbf{r}(t)$ and velocities $\mathbf{v}(t)$ to bending angle and impact parameter can be cast in many forms of which one is (Melbourne et al. 1994; Syndergaard, 1999)

$$d(t_i) = [v_{Rx} \cos \varphi(a_i) - v_{Tx} \cos \chi(a_i)] - \frac{dr_{RxTx}(t_i)}{dt} \quad (5)$$

$$\varphi(a_i) = \zeta - \arcsin\left(\frac{a_i}{r_{Rx}}\right) \quad (6)$$

$$\chi(a_i) = (\pi - \eta) - \arcsin\left(\frac{a_i}{r_{Tx}}\right) \quad (7)$$

$$\alpha(a_i) = \theta - \arccos\left(\frac{a_i}{r_{Rx}}\right) - \arccos\left(\frac{a_i}{r_{Tx}}\right) \quad (8)$$

a_i ... impact parameter at data sample i (time i)

α_i ... bending angle at data sample i

r_{Tx} ... distance of the transmitter (Tx) from the center of local curvature

r_{Rx} ... distance of the receiver (Rx) from the center of local curvature

r_{RxTx} ... distance between the transmitter and receiver satellite

v_{Tx} ... velocity of the transmitter satellite (in the occultation plane)

v_{Rx} ... velocity of the receiver satellite (in the occultation plane)

ζ ... angle between the Rx ray and position vectors (in the occultation plane)

η ... angle between the Tx ray and position vectors (in the occultation plane)

θ ... angle between the transmitter and the receiver position vectors

Eqs. (5) – (8) constitute the equation set used in the E5L processing, and Figure 4 illustrates the geometrical situation in the occultation plane, the plane spanned by the Tx and Rx satellite position vectors.

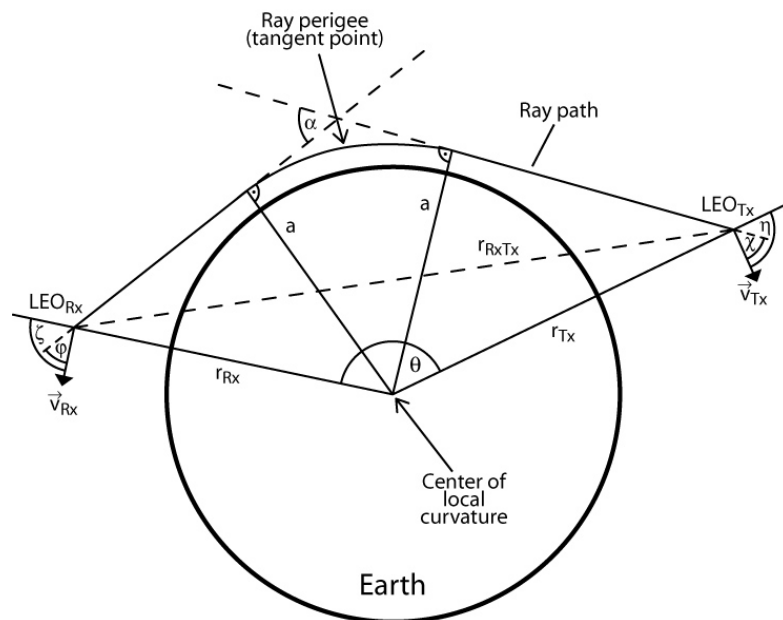


Figure 4: LEO-LEO occultation geometry, defining various parameters used in the algorithm description.

Eqs. (5) – (8) are used either with assuming a spherical Earth (with mean radius 6371.0 km) or a realistic ellipsoidal Earth shape (WGS-84 ellipsoid; e.g., Landolt-Börnstein, 1984). In the latter case, the transmitter and receiver position vectors $r_{Tx}(t)$ and $r_{Rx}(t)$ are first transformed to originate in the ellipsoid's center of local curvature in the occultation plane at the mean

geographic location of the event rather than in the Earth’s center of mass. The details of this “oblateness correction” have been described by Syndergaard (1998) (also included as App. C.2 in Syndergaard, 1999) and are not repeated here. The essence is that the position vector’s origin in the center of local curvature ensures that the assumption of spherical symmetry about the tangent point, implicit in Eqs. (6) – (8), is accurately valid geometrically.

A by-product of the correction is the knowledge of the mean tangent point location of the event (φ_{TP} , λ_{TP}) and of its radius of curvature at this location (R_C). In the spherical Earth case, the center of curvature and the center of mass are identical as are the radius of curvature and the Earth’s mean radius. The mean location (φ_{TP} , λ_{TP}) is computed, purely defined by geometry and independent of any atmospheric state, as the geographic location where the straight-line connection of Tx and Rx positions at a certain time during the event touches the ellipsoidal or spherical Earth’s surface. Experience with ray propagation through realistic atmospheres has shown this mean location to correspond to the location which real events typically reach near the tropopause at around 12 km, i.e., to be a very adequate mean location of any actual event though defined solely by geometry. The latter property offers the distinct advantage that purely geometrical analyses (e.g., on occultation event distributions and “true” atmospheric states at event locations) can be performed in strict consistence with forward modeling and retrieval analyses, which simulate occultation data for event locations of interest.

After the preparations described, the vectors $\mathbf{r}_{Tx}(t)$, $\mathbf{v}_{Tx}(t)$, $\mathbf{r}_{Rx}(t)$, $\mathbf{v}_{Rx}(t)$, which are utilized in the ECEF system in E5L processing, are converted by standard vector-analytical formulae to the scalar components $r_{Tx}(t)$, $v_{Tx}(t)$, $r_{Rx}(t)$, $v_{Rx}(t)$, which are the projections of the respective vectors onto the occultation plane. In case of the positions, which by definition lie in this plane, these are simply the vector magnitudes denoting the Tx and Rx distances from the Earth’s center of local curvature (see Figure 4). To complete the input required to Eqs. (5) – (8), the angles ζ , η , and θ and the straight-line distance $r_{RxTx}(t)$ are computed from standard vector formulae as well.

Eqs. (5) – (7) demand an iterative solution for a , since a is implicitly contained only. Starting with the straight-line impact parameter as first guess for a , an accurate solution is obtained within few iterations. Given a , α is readily computed via Eq. (8).

Statistical optimization of bending angles at high altitudes.

Statistical optimization optimally combines, in an inverse-covariance-weighted least-squares sense, the measured bending angle profile with a background bending angle profile and thereby ensures adequate quality of the bending angle profiles at high altitudes (from the stratosphere upwards) for the subsequent Abel transform to refractivity (subsection 3.3). Other more simplified methods exist to treat the upper boundary of bending angles before the Abel transform (see, e.g., Gobiet and Kirchengast, 2002, 2004; for an overview) but these are less effective and not treated here. The optimal estimation profile reads (e.g., Healy, 2001; Gobiet and Kirchengast, 2004)

$$\alpha_{opt} = \alpha_b + \mathbf{B}(\mathbf{B} + \mathbf{O})^{-1}(\alpha_o - \alpha_b) \quad (9)$$

- α_{opt} ... optimized bending angle profile
- α_o ... observed (retrieved) bending angle profile
- α_b ... background bending angle profile

\mathbf{O} ... observation error covariance matrix (of α_o)

\mathbf{B} ... background error covariance matrix (of α_b)

Eq. (9) assumes unbiased (Gaussian) errors and a linear problem. Linearity is fulfilled in the present case, and unbiasedness holds reasonably well for the retrieved profiles due to the self-calibrating nature of RO data (see above). Unbiasedness of background profiles needs careful selection of these profiles (Gobiet and Kirchengast, 2004).

In E5L processing, the optimization is applied from 30 to 120 km height. The error covariance matrices \mathbf{O} and \mathbf{B} are formulated as

$$\mathbf{O}_{ij} = \sigma_{oi}\sigma_{oj} \cdot \exp\left(-\frac{|a_i - a_j|}{L_o}\right), \quad \mathbf{B}_{ij} = \sigma_{bi}\sigma_{bj} \cdot \exp\left(-\frac{|a_i - a_j|}{L_b}\right) \quad (10)$$

a_i, a_j ... impact parameter for data samples i and j

σ_{oi}, σ_{oj} ... observation (retrieval) standard errors at levels i and j

σ_{bi}, σ_{bj} ... background standard errors at levels i and j

L_o ... correlation length of observation errors

L_b ... correlation length of background errors

The observation standard error is estimated from the 70–80 km height segment of a_o , where the SNR < 1, and assumed to hold for the full estimation range down to 30 km. L_o is set to 1 km in line with empirical evidence (e.g., Steiner and Kirchengast, 2004, 2005). The background standard error is set from experience to 15% of the α_b profile, and L_b is set to 6 km, as the smooth background profiles clearly have long-range correlation of the order of a scale height.

Suitable nearly unbiased α_b profiles are obtained from a profile search in the global MSIS90 (Hedin, 1991) or CIRA86aQ (Kirchengast et al., 1999) climatology with month-to-month 5 deg latitude \times 15 deg longitude search. The α_b profile selected is the one, which best fits the retrieved profile over the stratopause region (baseline: 45 to 65 km), where retrieved data quality is still sufficiently good to allow a reasonable fit. The best-fit profile is then used up to 120 km and ensures that, via Eq. (9), a reasonable optimized bending angle profile α_{opt} is available up to 120 km, independent of the retrieved data reaching an SNR < 1 at heights of about 80 km (e.g., Rieder and Kirchengast, 2001a). This is vital for the subsequent Abel transform to induce only small error propagation from the mesospheric altitudes into the retrieval domain of interest below the stratopause (e.g., Gobiet and Kirchengast, 2002). Below about 40 km, the influence of the background profile is negligible since from the middle stratosphere downwards the retrieved data exhibit an SNR \gg 1 so that Eq. (9) directly yields α_o for α_{opt} . Gobiet and Kirchengast (2004) describe the ingredients of careful statistical optimization in detail.

The outputs of the bending angle retrieval are α_i (α_{opt} from Eq. 9), a_i , R_C , and $(\varphi_{TP}, \lambda_{TP})$, which are used in the subsequent processing steps.

3.2. Transmission Retrieval

Transmission retrieval starts with the amplitude profiles at each signal frequency j , $A_j(t)$, and derives transmission profiles as function of impact parameter $Tr_j(a)$, which expresses atmospheric absorption (transmission = 1 – absorption) at frequency j due to water vapor and the background air (molecular oxygen and nitrogen). The transmission retrieval comprises three steps:

- defocusing and spreading correction
- amplitude normalization
- differential transmission computation (if chosen)

Defocusing and spreading correction.

This correction is required since $A_j(t)$ contains besides the desired amplitude loss due to absorption also defocusing loss due to differential bending and spherical signal spreading according to the geometry (e.g., Leroy, 2001).

Both defocusing and spreading can be corrected for in using the bending angle retrieval output (see subsection 3.1), namely the bending angle profile $\alpha(a)$ or, alternatively, the satellite opening angle $\theta(a)$ (see Figure 4) and the impact parameter profile a as well as the Tx and Rx satellite radial distances $r_{Tx}(a)$ and $r_{Rx}(a)$. Different variants for this correction exist (e.g., Sokolovskiy, 2000; Leroy, 2001; Jensen et al., 2003). In E5L processing the elegant one-step formulation of Jensen et al. (2003) for the defocusing and spreading model amplitude (for GO processing) is used which reads

$$A_{dsm}(a_i) = \left[\frac{a_i}{(r_{Tx} r_{Rx})^2 \sin(\theta) \sqrt{1 - \left(\frac{a_i}{r_{Tx}}\right)^2} \sqrt{1 - \left(\frac{a_i}{r_{Rx}}\right)^2} \left| \frac{d\theta}{da} \right|_i} \right]^{1/2} \quad (11)$$

$\left| \frac{d\theta}{da} \right|_i$... derivative of the satellite opening angle (Figure 4) after the impact parameter at level i

A_{dsm} ... defocusing and spreading model amplitude

Different formulations have to be used for WO pre-processed amplitudes (Jensen et al., 2003; Nielsen et al., 2005). $A_{dsm}(a_i)$ can be used in a next step as correction to convert the observed amplitude $A_j(t) = A_j(a)$ to the desired transmissions $Tr_j(a)$.

Amplitude normalization.

$Tr_j(a)$ being a normalized intensity, $A_j(t)$ has to be divided in some way by a normalization amplitude at some reference height besides removing the defocusing and spreading components. In E5L processing the derivation of $Tr_j(a)$ is done via

$$A_j^{dsm}(a_i) = \left(\frac{A_j}{A_{dsm}} \right)_{z_{ref j}}^{\Delta z} \cdot A_{dsm}(a_i) \quad (12)$$

$$Tr_j(a_i) = -20 \cdot (\log A_j - \log A_j^{dsm}) \text{ [dB]} \quad (13)$$

$\left(\frac{A_j}{A_{dsm}} \right)_{z_{ref j}}^{\Delta z}$... absorption amplitude at reference height $z_{ref j}$ for frequency j
(mean estimate over a height range $\pm \Delta z/2$ about $z_{ref j}$)

A_j^{dsm} ... defocusing and spreading model amplitude scaled to match the signal amplitude A_j at height $z_{ref j}$

Eq. (12) performs the normalization in that it scales $A_{dsm}(a_i)$ to $A_j(a)$ at $z_{ref j}$ and Eq. (13) then performs the division $A_j(a)/A_j^{dsm}$, corresponding to a subtraction in [dB] space, to obtain the desired transmissions $Tr_j(a)$ pertaining to absorption only. $Tr_j(a)$ above $z_{ref j}$ is set to zero.

The $z_{ref j}$ baseline value used for the ACE+ type signal frequencies is 25 km or 30 km, since from about 25 km upwards $Tr_j(a)$ is unity (zero absorption) with high accuracy. This normalization to a reference height “above the absorptive atmosphere” where $Tr_j(a) = 1$ is the step where the intrinsic self-calibration of the amplitudes comes in: as for the self-calibrated bending angles it implies that as long as the transmission profiles are short-term stable over the ~30 sec of the occultation event from about 30 km towards the surface, each individual profile is a self-standing reliable measure of the atmospheric absorption at frequency j at the given place and time, independent of any other real or potential measurements before, in parallel, or after the ~30-sec event. As will be seen in subsection 3.4 below, the imaginary refractivity (or absorption coefficient) derived from the transmission only depends on the derivative $d \ln Tr_j(a) / da$, so that a small constant transmission residual at height $z_{ref j}$ does not matter.

In E5L processing also filtering is involved, smoothing a before use in Eq. (11) as well as $A_j(a)$ and $A_{dsm}(a)$ before use in Eqs. (12) and (13). A 3rd order polynomial filter was found adequate for this purpose with the filtering polynomial width set to ~1 km. The transmission profiles $Tr_j(a)$ are smoothed the same way. Similar to the phase delay filtering before Doppler shift deduction (subsection 3.1), this filtering avoids unnecessary amplification of high-frequency noise in the subsequent Abel transform to imaginary refractivity, which involves the derivative of $Tr_j(a)$ being similarly noise-sensitive as the phase delay derivation.

Differential Transmission Computation (if chosen).

If the subsequent processing steps are foreseen to start with differential transmissions, instead of with the direct transmissions $Tr_j(a)$, the log-transmission difference, $\ln Tr_{jk}(a) = \ln Tr_j(a) - \ln Tr_k(a)$, is computed for any pair of frequencies f_j and f_k (e.g., f_{12}, f_{23} for an ACE+ type three-frequency system). The obtained differential transmission profiles, $Tr_{jk}(a)$, the number of which is due to the differencing always one less than the number of direct transmission profiles $Tr_j(a)$, are then fed into the subsequent imaginary refractivity retrieval step, which in this case leads to differential imaginary refractivity profiles (and differential absorption coefficients).

Since the formulae and algorithms of the subsequent processing are identical for either $Tr_{jk}(a)$ or $Tr_j(a)$ profiles as input (except that there is one less profile fed in if using $Tr_{jk}(a)$), we do not separately repeat the equations applying to $Tr_{jk}(a)$. It is rather to be understood that $Tr_j(a)$ always means $Tr_{jk}(a)$ in case differential transmissions are employed. Reflecting this, also in the E5L processing each differential transmission profile $Tr_{jk}(a)$ is assigned to frequency j , so that formally it is treated subsequently in an identical way as $Tr_j(a)$. The highest frequency (e.g., f_3 in an ACE+ type system) is left spare in this case, however, and the retrieval proceeds with one frequency less.

In the descriptions below this aspect of optionally processing differential profiles is generally indicated with including the optional word “(differential)” as adjective to transmission, and in an analogous way, also as adjective to imaginary refractivity and to absorption coefficient, respectively.

The key rationale for potentially using differential transmission instead of direct transmission profiles for LRO data processing lies in the strong mitigation of scintillations due to atmospheric turbulence that are possible when an adequate wave-optics based bending angle and transmission retrieval processing is run based on which the differential transmission profiles are then prepared. Details on this are found in Gorbunov and Kirchengast (2005a,b) as well as in Gorbunov and Kirchengast (2006).

3.3. Real Refractivity Retrieval

The real refractivity profile as function of height is derived from the bending angle profile as function of impact parameter via the classical Abel transform (e.g., Fjeldbo et al., 1971; Kursinski et al., 1997; Rieder and Kirchengast, 2001b)

$$n^R(a_i) = \exp\left(\frac{1}{\pi} \int_{a_i}^{a_{Top}} \frac{\alpha(a)}{\sqrt{a^2 - a_i^2}} da\right) \quad (14)$$

$$N^R(z_i) = 10^6(n^R(a_i) - 1), \quad z_i = r_i - R_C, \quad r_i = \frac{a_i}{n^R(a_i)} \quad (15)$$

- n^R ... refractive index, real part
- r_i ... radial distance of level a_i from center of local curvature
- z_i ... ellipsoidal height level corresponding to a_i
- N^R ... real refractivity

In E5L processing, the top value a_{Top} of the Abelian integral, Eq. (14), which is at infinite heights theoretically (e.g., Fjeldbo et al., 1971), is set to correspond to a height of 120 km, exploiting the bending angle profile available from Eq. (9) over the full range and ensuring accurate refractivity retrieval up to the stratopause (Steiner et al., 1999). The value at the top is, to have a sensible physical value instead of zero, set to the refractivity (more precisely to $n^R - 1$) of MSIS90 at 120 km, though its effect relative to being zero is negligible in $N^R(z_i)$ below the stratopause. In Eq. (15) it is vital to use exactly the R_C value used already in the bending angle retrieval (subsection 3.1) in order to ensure accurate ellipsoidal heights z_i .

3.4. Imaginary Refractivity/Absorption Coefficient Retrieval

The (differential) imaginary refractivity profile as function of height is derived by using the real refractive index profile and the impact parameter profile together with the (differential) transmission profiles of each signal frequency (pair) within another Abel transform akin to Eq. (14) (e.g., Kursinski et al., 2002)

$$k_j(z_i) = \frac{1}{\pi} \left| \frac{da}{dr} \right|_{a=a_i} \int_{a_i}^{a_j^{Top}} \frac{d \ln Tr_j(a)}{da} \frac{1}{\sqrt{a^2 - a_i^2}} da \quad (16)$$

$$N_j^I(z_i) = 10^6 \cdot \frac{c}{4\pi f_j} k_j(z_i) \quad (17)$$

$Tr_j(a)$... transmission profile at frequency j (dimension less units)

k_j ... (diff.) absorption coefficient at freq. j at level z_i , corresponding to a_i (cf. Eq. 15)

f_j ... frequency at frequency channel j

c ... velocity of light (in vacuum) ($c = 299792458$ m/s)

N_j^I ... (differential) imaginary refractivity at frequency j at level z_i

The real refractivity information enters via the radial distance profile $r(n^R)$ evaluated according to Eq. (15), which is needed to form the derivative $|da/dr|$ in Eq. (16). Eq. (17) is the standard equation for converting the (differential) absorption coefficient to (differential) imaginary refractivity (e.g., Schanda, 1986) to which it is proportional via the wavelength λ_j ($\lambda_j = c/f_j$).

In E5L processing, the top value a_j^{Top} of the Abelian integral Eq. (16), which is at infinite heights theoretically, is set to correspond to a height of $z_{refj} + \Delta z/2$ (as defined for Eq. (12)). Above this height the log-transmission $\ln Tr_j(a)$ and thus its integral contribution is zero.

After retrieval of the $N_j^I(z)$ profiles via Eq. (17) at each frequency j , they are filtered with a 3rd order polynomial filter with the filtering polynomial width set to ~ 1 km. As for the Doppler shift and transmission profile above, this filtering avoids potential high-frequency noise incurred by application of Eq. (16) to be transferred to further exploitation of $N_j^I(z)$ such as in the subsequent atmospheric profiles retrieval.

3.5. Atmospheric Profiles Retrieval

Real refractivity $N^R(z)$ and (differential) imaginary refractivities $N_j^I(z)$ are used, together with the equations relating atmospheric pressure p , temperature T , humidity q , and cloud liquid water lw to $N^R(z)$ and $N_j^I(z)$, to derive the parameters p , T , q , and lw as function of height z . In addition, the geopotential height of pressure levels, $Z(p)$, can be obtained from the knowledge of the $p(z)$ profile. The key equations involved and used in E5L processing are

- the real refractivity equation (E5L: Smith-Weintraub equation; e.g., Foelsche, 1999),

$$N^R(z) = 77.60 \frac{p(z)}{T(z)} + 3.73 \cdot 10^5 \frac{e(z)}{T(z)^2} \quad (18)$$

p ... total air pressure [hPa]
 e ... total water vapor partial pressure [hPa]
 T ... temperature [K]
 N^R ... real refractivity

- a complex (real and imaginary) refractivity model and its adjoint model (E5L: Advanced MPM93 Model and its adjoint; e.g., Liebe et al., 1993; Nielsen et al., 2005; Giering and Kaminski, 1998),

$$(N^{R\text{mod}}(z), N_j^{I\text{mod}}(z)) = N_j^{C\text{mod}}(f_j, p(z), T(z), e(z), lw(z), iw(z), rr(z)) \quad (19)$$

$$(K^{R\text{adj}}(z), K_j^{I\text{adj}}(z)) = K_j^{C\text{adj}}(f_j, p(z), T(z), e(z), lw(z), iw(z), rr(z)) \quad (20)$$

lw, iw, rr ... cloud liquid water, cloud ice water, rain rate
 $N^{R\text{mod}}$... modeled real refractivity
 $N_j^{I\text{mod}}$... modeled imaginary refractivity

$$\mathbf{K}^{R\text{adj}} = \left(\frac{\partial N^R}{\partial T}, \frac{\partial N^R}{\partial e}, \frac{\partial N^R}{\partial lw} \right)^T \dots \text{modeled real refractivity Jacobians}$$

$$\mathbf{K}_j^{I\text{adj}} = \left(\frac{\partial N_j^I}{\partial T}, \frac{\partial N_j^I}{\partial e}, \frac{\partial N_j^I}{\partial lw} \right)^T \dots \text{modeled imag. refractivity Jacobians}$$

- the hydrostatic equation with the equation of state in moist air embedded (e.g., Salby, 1996),

$$\frac{d \ln p(z)}{dz} = - \frac{g(z)}{R^d T_v(z)} \quad (21)$$

R^d ... dry air gas constant ($R^d = 287.06 \text{ J kg}^{-1} \text{ K}^{-1}$)
 g ... acceleration of gravity (standard $g(z, \text{latitude})$ model; e.g., Gobiet and Kirchengast, 2002)
 T_v ... virtual temperature (see Eq. (22))

- and the equations for virtual temperature and conversion of water vapor pressure to specific humidity (e.g., Salby, 1996),

$$T_v(z) = T(z) \cdot (1 + 0.608 q(z)) \quad (22)$$

$$q(z) = 0.622 \frac{e(z)}{(p(z) - 0.378 e(z))} \quad (23)$$

Eqs. (18) and (21)–(23) are well-known fundamental equations of atmospheric physics, Eqs. (19) and (20) are a macroscopic expression of a more sophisticated spectroscopic model. The essence of the Advanced MPM93 Model, Eq. (20), for the present purpose is simple, however: it provides for any physically realistic local atmospheric state (p, T, e, lw, iw, rr) and any given X/K band signal frequency j the corresponding complex refractivity $(N^{R\text{mod}}, N^{I\text{mod}}_j)$. $N^{R\text{mod}}$ is modeled for the retrieval such that $N^{R\text{mod}}$ equals N^R of Eq. (18), i.e., according to the “Smith-Weintraub” formulation (Smith and Weintraub, 1953; Foelsche, 1999).

Since the atmospheric profiles retrieval as described below requires knowledge also of the sensitivities (“Jacobians”; e.g., Rodgers, 2000) of (N^R, N^I_j) to the atmospheric state parameters (T, e, lw) at any given state (p, T, e, lw, iw, rr) , also the adjoint model $\mathbf{K}^{Cadj}(f_j, p, T, e, lw, iw, rr)$ is used, the source code of which was generated in an automatic way from the source code of the model $N^{Cmod}_j(f_j, p, T, e, lw, iw, rr)$ by the Tangent-Linear and Adjoint Model Compiler TAMC (Giering and Kaminski, 1998). The Jacobians are accurate for any given state since the Advanced MPM93 model is locally linear in the neighborhood of any given state despite being non-linear if viewed over its complete relevant state space. If retrieved differential imaginary refractivity profiles are available, due to the differential transmission retrieval approach being used, both the modeled imaginary refractivities and the modeled Jacobians are differenced between the appropriate frequency pairs so that they correctly match the retrieved differential imaginary refractivities in the BLUE algorithm described below.

The problem of retrieving the atmospheric state (p, T, e, lw) from the refractivities (N^R, N^I_j) is efficiently solved by downward (in height) integration of the hydrostatic equation, Eq. (21), to sequentially obtain p , combined with an iterative BLUE (best linear unbiased estimation) solution at each integration step to obtain (T, e, lw) from (N^R, N^I_j) (recall Figure 3 in section 2.2 above for a schematic overview).

The downward integration of Eq. (21) is initialized at high altitudes (E5L setting: 75 km) with some initial state $(p_{Top}, T_{Top}, e_{Top} = lw_{Top} = 0)$, the accuracy of which is non-critical as any initialization errors decay quickly over the first about 3 scale heights, i.e., essentially within the mesosphere (E5L baseline: estimate of (p_{Top}, T_{Top}) from the local scale height estimated from $N^R(z)$ near 75 km and the local equation of state). 4th order Runge-Kutta integration of Eq. (21) is used (e.g., Gershenfeld, 1999; chapter 6 therein) with small integration steps (E5L setting: 100 m) to ensure accurate $p(z_i)$ values. This integration itself involves already the BLUE algorithm described below, in order to obtain, for the needed Runge-Kutta sub-steps, $T_v(z)$ in Eq. (21) from states (T, e, lw) estimated from (p, N^R, N^I_j) .

After each integration step, using the value of p^i obtained at height z_i and the estimated state $(T^{i+1}, e^{i+1}, lw^{i+1})$ from the previous height z_{i+1} , the BLUE algorithm is run to obtain the state

(T^i, e^i, lw^i) from the data (p^i, N^{Ri}, N^{Ij}) at height z_i . The pressure p^i acts as a useful “backbone” for this estimation and ensures it to be very robust and reliable. Practically, above a certain height z_{eTop} , above which water vapor has negligible effect, only T^i is estimated (E5L baseline: 20 km). Furthermore, above a certain height z_{lwTop} , above which liquid water density is negligible, only (T^i, e^i) is estimated (E5L baseline: 8.5 km). Below z_{lwTop} the full state (T^i, e^i, lw^i) is estimated, which then requires at least 3 independent elements of information in (p^i, N^{Ri}, N^{Ij}) .

For the BLUE solution, an iterative Gauss-Newton algorithm of the following form is used (e.g., Rodgers, 2000; chapter 5.3 therein):

$$\mathbf{x}_{n+1} = \mathbf{x}_n + (\mathbf{K}_n^T \cdot \mathbf{C}_y^{-1} \cdot \mathbf{K}_n + \mathbf{C}_b^{-1})^{-1} [\mathbf{K}_n^T \mathbf{C}_y^{-1} (\mathbf{y} - \mathbf{y}^{\text{mod}}(\mathbf{x}_n)) - \mathbf{C}_b^{-1} (\mathbf{x}_n - \mathbf{x}^b)] \quad (24)$$

$$\mathbf{y} = (N^R, N_j^I)^T, \quad \mathbf{y}^{\text{mod}} = (N^{R\text{mod}}, N_j^{I\text{mod}})^T \quad (25)$$

$$\mathbf{C}_y = \text{Diag}(\sigma_{N^R}^2, \sigma_{N_j^I}^2) \quad (26)$$

$$\sigma_{N^R} = \begin{cases} N^R [f_{15} \cdot \exp(f_{hi}(z - 15\text{km}))] & \text{for } z \geq 15\text{km} \\ N^R \left[f_{15} + f_{lo} \left(\frac{1}{\text{Max}(z, 1\text{km})} - \frac{1}{15\text{km}} \right) \right] & \text{for } z < 15\text{km} \end{cases} \quad (27)$$

$$\sigma_{N_j^I} = \sigma_{N_j^I}^0 \cdot \left[f_w \cdot \left(\frac{1}{\text{Max}(Tr_j(z_i), 10^{-6})} + f_c \cdot \frac{1}{\text{Max}(Pt_j(z_i), 10^{-6})} \right) \right] \cdot f_{T^{\text{fit}}} \quad (28)$$

$$\mathbf{K} = (\mathbf{K}^{R\text{adj}}, \mathbf{K}_j^{I\text{adj}})^T \quad (29)$$

$$\mathbf{x} = (T, e, lw)^T, \quad \mathbf{x}^b = \mathbf{x}(z_{i+1}) = (T^b, e^{i+1}, lw^{i+1})^T, \quad \mathbf{x}_0 = \mathbf{x}^b \quad (30)$$

$$T^b = \begin{cases} T^{i+1} & \text{for } z > z_{\text{thres}} \\ T^{\text{fit}} & \text{for } z < z_{\text{thres}} \end{cases} \quad (31)$$

$$\mathbf{C}_b = \text{Diag}(\sigma_T^2, \sigma_e^2, \sigma_{lw}^2) \quad (32)$$

$$\sigma_T = \begin{cases} \text{const. for } z > z_{\text{thres}} \\ s_T^{z_{\text{thres}}} + \left(\frac{ds_T}{dz} \right) |z - z_{\text{thres}}| & \text{for } z < z_{\text{thres}} \end{cases}; \quad \sigma_e, \sigma_{lw} = \text{const.} \quad (33)$$

- n ... iteration index for the iterative BLUE estimator ($n = 0, \dots, \text{Min}(n_{\text{converged}}, 12)$)
- \mathbf{y} ... measurement vector (real and (diff.) imag. refractivities; baseline from ACE+ $j = 1, 2, 3$, i.e., four elements N^R, N_1^I, N_2^I, N_3^I , resp. three if differential N_1^I, N_2^I)

- \mathbf{y}^{mod} ... forward modeled measurement vector, updated at each iteration n (from call of Advanced MPM93 Model Eq. (19))
- \mathbf{C}_y ... measurement (and forward modeling) error covariance matrix (set as diagonal matrix)
- σ_{N^r} ... standard error of real refractivity (formulation following Steiner and Kirchengast, 2005; baseline E5L parameters: $f_{15} = 0.001$, $f_{hi} = 0.02$, $f_{lo} = 0.01$)
- $\sigma_{N_j^i}$... standard error of imaginary refractivity at frequency j
- $\sigma_{N_j^i}^0$... standard error estimate for N_j^i within the $z_{refj} \pm \Delta z/2$ height range (cf. Eq. (12))
- Pt_j ... amplitude *rms* error estimate from high-pass filtered data (with ~ 1 km filter bandwidth) for optional up-scaling of $\sigma_{N_j^i}$ in presence of scintillations (f_C is set to switch this term to unity if the optional up-scaling shall be disabled)
- f_w ... weighting factor (baseline E5L setting is to unity)
- $f_{T^{fit}}$... factor with nominal value of unity; if $z_i < z_{thres}$ $f_{T^{fit}}$ set to $\text{Min}(5 + 2.5 \cdot |z_i - z_{thres}|[\text{km}], 10)$ (baseline E5L setting to down-weight N_j^i influence on the estimated \mathbf{x})
- \mathbf{K} ... Jacobian weighting matrix (dimension: no. of elements in $\mathbf{y} \times$ no. of elements in \mathbf{x}), updated at each iteration n (from call of adjoint model to Advanced MPM93 Model, Eq. (20))
- \mathbf{x} ... state vector to be estimated, updated at each iteration n
- \mathbf{x}^b ... background (a priori) state vector (set nominally to state of previous state estimate on previous height level z_{i+1})
- \mathbf{x}_0 ... initial guess state vector (used as starting point for iteration of Eq. (24))
- T^b ... background (a priori) temperature, given $z_{thres} > z_0$ (bottom level of profile) a “best-fit background profile” temperature T^{fit} is used at $z_i < z_{thres}$ instead of T^{i+1} from previous height level z_{i+1}
- \mathbf{C}_b ... background (a priori) error covariance matrix (set as diagonal matrix)
- $\sigma_T, \sigma_e, \sigma_{lw}$... standard errors of temperature, water vapor pressure, liquid water density (set nominally to high values so that the influence of the background state \mathbf{x}^b on the estimated \mathbf{x} is negligible; given T^{fit} at $z_i < z_{thres}$ is used, σ_T is set to a smaller standard error consistent with the uncertainty of $T^{fit}(z_i)$ so that in this case – and only in this case – T^b exerts influence on the estimated \mathbf{x})
- $s_T^{z_{fit} \min}$... background standard error estimate for best-fit profile temperature at level z_{thres} (baseline E5L setting: 0.75 K)
- $\left(\frac{ds_T}{dz}\right)$... downward increase of background standard error estimate with increasing distance from z_{thres} (baseline E5L setting: 0.25 K/km)
- z_{thres} ... threshold height for $N_j^i(z_i)$ quality below which a best-fit background temperature T^b is enabled to exert influence on \mathbf{x} ; above influence of background \mathbf{x}^b is negligible

Because the estimation problem is slightly over-determined for the ACE+ type baseline of three signal frequencies (two frequencies if differential transmission retrieval approach), it is possible to retrieve the state (T^i, e^i, lw^i) even if one of the independent information pieces is lost, as will frequently be the case at any given height level, where only two of the three frequencies provide amplitude data in a useful dynamic range. Even if, for example, the information from two imaginary refractivities (or one differential imaginary refractivity) is lost, which can happen for example in very wet regions, pressure, humidity and temperature still can be calculated if concentration of liquid water can be neglected or some information component (e.g., temperature) is known to some degree from background data. Information of real refractivity at lowest ACE+ type frequency (near 10 GHz) will get lost only in extreme (and rare) situations, in which case the retrieval in the lower troposphere is compromised.

If the imaginary refractivity variances grow large enough into the lower troposphere so as to render the BLUE problem effectively underdetermined, which can happen in case of atmospheric turbulence, the advanced processing approaches described below will be used. The first one is applicable in case of direct transmission retrieval, the second one in case of differential transmission retrieval. We note that the second one is clearly favorable in presence of strong turbulence, since it avoids invoking auxiliary a priori information.

Processing data from direct transmission retrieval in case of severe turbulence.

Strong amplitude scintillations due to atmospheric turbulence can introduce significant noise into the imaginary refractivity data and may degrade the above baseline retrieval of atmospheric profiles below about 3 to 6 km in the troposphere. However, since the parts of the signal affected by scintillation can be identified due to the high sampling rate of the raw measurements (1 kHz), this enables a constant monitoring of the high frequency fluctuations and the determination of a “threshold height”, z_{thres} , below which the imaginary refractivity data should be used with caution and receive low to negligible weight in the BLUE process (cf. Eqs. (31)–(33)). As turbulence is a layered phenomenon (e.g., Gage, 1990), usually only some fraction of the height levels below z_{thres} may need to receive such down-weighting, but it will generally be difficult to determine this in real time. Thus in E5L processing it is assumed, as a conservative limit, that the complete height range below any z_{thres} found is filled with turbulence and is down-weighted (Eq. (33)).

In case of down-weighting applied to imaginary refractivities below z_{thres} , one sensible way to cure the consequent under-determination of the BLUE problem is to introduce weak background (a priori) information into the retrieval at the height levels concerned. The primary candidate information for this purpose is temperature, since it is well predictable in the troposphere above the boundary layer and since it is sufficient auxiliary information under all conditions to ensure a robust estimation. Suitable background temperature profiles (T_b) can be obtained from a profile search in an adequate database (e.g., from a 24h ECMWF forecast in a geographic area of some degrees around the profile co-located with the measurement). The T_b profile selected can be the one that best fits the retrieved temperature profile in the troposphere right above z_{thres} , where the retrieved data are still very accurate and allow for a good fit. The fit to the retrieved data, and not just selection of a co-located profile, is to avoid importing any potential small bias from the background into the retrieval (though ECMWF temperatures below 8 km are essentially unbiased). In E5L processing, exactly this “best-fit T extrapolation” approach is used for heights below z_{thres} (cf. Eq. (31) and Figure 3, section 2.2)

and found to ensure accurate humidity and temperature retrieval also under severe turbulence conditions.

Processing data from wave-optics based differential transmission retrieval in case of severe turbulence.

Wave-optics approaches (e.g., Canonical Transform, Gorbunov (2002a,b); Full Spectrum Inversion; Jensen et al. (2003)), can be used to reduce scintillation fluctuations already on the transmission measurements (Level 1b) so that down-weighting of imaginary refractivity data will be avoided at the atmospheric profiles retrieval step. As pioneered by Gorbunov and Kirchengast (2005a,b; 2006), it is in particular the use of differential transmission profiles, which are preceded in processing by a Canonical Transformation step, that enable accurate atmospheric profiles retrieval into the lower troposphere without prior information also in case of severe turbulence. In other words, the threshold Z_{thres} will in general only be reached close to the boundary layer, where the signal attenuation becomes so strong so as to anyway limit the retrieval penetration by low SNR conditions.

The upgraded E5L processing, upgraded by use of the algorithms described by Gorbunov et al. (2006) in the companion report from Tasks 1.1 and 1.2 of the Prodex-CN1 project, includes now a wave-optics based bending angle and transmission retrieval capability, which delivers differential transmission profiles of a quality so that the subsequent differential imaginary refractivity and atmospheric profiles retrieval is able to obtain high quality temperature and humidity profiles also in case of severe turbulence without need to invoke the “best-fit T extrapolation” approach.

4. Summary and Conclusions

This report provided, after a brief overview on the EGOPS5 software and on the structure and elements of its LRO retrieval processing chain, an in-depth description of the processing chain and retrieval algorithms after the advancements by the Prodex-CN1 Project.

The bending angle and transmission retrieval part was in this report described for the geometric-optics data processing approach. The cited companion report by Gorbunov et al. (2006) provides a detailed description of the wave-optics based bending angle and transmission retrieval, advancing a baseline description by Gorbunov and Kirchengast (2005a,b).

The report will be of significant utility also beyond the algorithmic documentation of the EGOPS5 LRO processing chain, since it is the so far most detailed description of LRO retrieval algorithms also in a generic sense. It thus provides valuable information for anyone interested to learn about LRO processing in more depth than covered by other sources.

The EGOPS5 LRO retrieval system itself is now at an advanced level enabling flexible processing in both direct and differential transmission retrieval modes, and using at the bending angle and transmission retrieval step either a wave-optics or geometric-optics based approach, respectively. Future advancements of LRO processing in EGOPS shall thus be targeted at further integration (at system and module level) with GRO processing, and in particular at integration with upcoming LEO-LEO IR laser occultation (LIO) retrieval capabilities related to the new mission concept ACCURATE (Kirchengast and Schweitzer, 2006).

Acknowledgments. The authors thank J. Ramsauer, U. Foelsche, A. Gobiet, M. Borsche, and A.K. Steiner (all WegCenter/UniGraz) for their many valuable contributions to the EGOPS5 software. The EGOPS5 software, the core tool underlying the processing chain and algorithms descriptions of this report, was developed by an international consortium led by UniGraz and involving partner teams at Danish Meteorological Institute, Denmark, Chalmers University of Technology, Sweden, and University of Bremen, Germany, and also all colleagues in these partner teams are thanked for their important contributions. EGOPS5 is based on strong heritage from EGOPS4, which was developed 1996–2003 by a consortium led by UniGraz and involving partner teams at Danish Meteorological Institute and TERMA Elektronik A/S, Denmark, the Met. Office, U.K., and Austrian Aerospace GmbH, Austria, with the major funding provided by the European Space Agency. The major funding for the recent advancements of EGOPS5 LRO processing 2005–2006 was provided by the European Space Agency under the Prodex-CN1 project. Furthermore, co-funds for part of the advancements came from the Austrian Science Fund FWF (START Programme No. Y103-N03, Project P18837/CLIMROCC) and the Austrian Aeronautics and Space Agency of the Austrian Research Promotion Agency FFG-ALR (ACCURAIID Project).

References

- Budden, K.G.**, The propagation of radio waves - The theory of radio waves of low power in the ionosphere and magnetosphere, Cambridge Univ. Press, Cambridge, U.K., 1985.
- Fjeldbo, G., A. Kliore, and V.R. Eshleman**, The neutral atmosphere of Venus as studied with the Mariner V radio occultation experiments, *Astron. J.*, 76, 123-140, 1971.
- Foelsche, U.**, Tropospheric water vapor imaging by combination of ground-based and spaceborne GNSS sounding data (Ph.D. thesis), *Wissenschaftl. Ber. No. 10*, 164 p., Inst. Meteorol. Geophys., Univ. of Graz, Austria, 1999.
- Gage, K.S.**, Radar Observations of the Free Atmosphere: Structure and Dynamics, in *Radar in Meteorology (ed. D. Atlas), part II, chap 28*, American Met. Society (AMS) Publ., 534-565, 1990.
- Giering, R., and T. Kaminski**, Recipes for Adjoint Code Construction, *ACM Trans. On Math. Software*, 24, 437-474, 1998.
- Gobiet, A., and G. Kirchengast**, Sensitivity of atmospheric profiles retrieved from GNSS occultation data to ionospheric residual and high-altitude initialization errors, *Techn. Report for ESA/ESTEC No. 1/2002*, Inst. for Geophys., Astrophys., and Meteorol., Univ. of Graz, Austria, 2002.
- Gobiet, A., and G. Kirchengast**, Advancements of GNSS radio occultation retrieval in the upper stratosphere for optimal climate monitoring utility, *J. Geophys. Res.*, 109, D24110, doi: 10.1029/2004JD005117, 2004.
- Gorbunov, M.E.**, Canonical transform method for processing GPS radio occultation data in the lower troposphere, *Radio Sci.*, 37, 9-1–9-10, doi: 10.1029/2000RS002592, 2002a.
- Gorbunov, M.E.**, Radio-holographic analysis of Mircrolab-1 radio occultation data in the lower troposphere, *J. Geophys. Res.*, 107, 7-1–7-10, doi: 10.1029/2001JD000889, 2002b.
- Gorbunov, M.E., and G. Kirchengast**, Advanced wave-optics processing of LEO-LEO radio occultation data in presence of turbulence, *Tech. Rep. ESA/ESTEC-1/2005*, IGAM, Univ. of Graz, Austria, 2005a.

- Gorbunov, M.E., and G. Kirchengast,** Processing X/K band radio occultation data in the presence of turbulence, *Radio Sci.*, 40, RS6001, doi: 10.1029/2005RS003263, 2005b.
- Gorbunov, M.E., and G. Kirchengast,** Influence of anisotropic turbulence on X/K band radio occultation signals and related transmission retrieval quality, *Prodex-CN1 Task 2.2 Report to ESA/ESTEC-draft vers.Jul06*, Wegener Center, Univ. of Graz, Austria, 2006.
- Gorbunov, M.E., G. Kirchengast, and K.B. Lauritsen,** Advanced wave-optics forward modeling and bending angle and transmission retrieval including turbulent random refractivity field modeling, *Tech. Rep. ESA/ESTEC-1/2006*, Wegener Center, Univ. of Graz, Austria, 2006.
- Healy, S.B.,** Smoothing radio occultation bending angles above 40 km, *Ann. Geophys.*, 19, 459-468, 2001.
- Hedin, A.E.,** Extension of the MSIS thermosphere model into the middle and lower atmosphere, *J. Geophys. Res.*, 96, 1159-1172, 1991.
- Jensen, A.S., M. Lohmann, H.-H. Benzon, and A. Nielsen,** Full spectrum inversion of radio occultation signals, *Radio Sci.*, 38, 763, doi: 10.1029/2002RS002, 2003.
- Kirchengast, G., J. Hafner, and W. Poetzi,** The CIRA86aQ_UoG model: An extension of the CIRA-86 monthly tables including humidity tables and a Fortran95 global moist air climatology model, *Techn. Report for ESA/ESTEC No. 8/1999*, Inst. Meteorol. Geophys., Univ. of Graz, Austria, 1999.
- Kirchengast, G., J. M. Fritzer, M. Schwärz, S. Schweitzer, and L. Kornblueh,** The Atmosphere and Climate Explorer Mission ACE+: Scientific Algorithms and Performance Overview. *Techn. Rpt. for ESA/ESTEC No. 2/2004*, IGAM, Univ. of Graz, Austria, 2004a.
- Kirchengast, G., S. Schweitzer, J. Ramsauer, and J. Fritzer,** End-to-end Generic Occultation Performance Simulator Version 5 (EGOPS5) Software User Manual (Overview-, Reference-, and File Format Manual), *Tech. Rep. for ESA/ESTEC No. 6/2004*, Inst. for Geophys., Astrophys., and Meteorol., Univ. of Graz, Austria, 2004b.
- Kirchengast, G., and S. Schweitzer,** ACCURATE LIO Initial Assessment Project: Breadboard Studies and Scientific Studies – Requirements, Concepts, Investigations, and Results, *Doc.Id. WegC/ACCURATE/LIO-IAP/Jul06/1*, Report supported by the FFG-ALR project ACCURAD, 28 pp, Wegener Center, Univ. of Graz, Austria, 2006.
- Kursinski, E.R., G.A. Hajj, J.T. Schofield, R.P. Linfield, and K.R. Hardy,** Observing Earth's atmosphere with radio occultation measurements using the Global Positioning System, *J. Geophys. Res.*, 102, D19, 23429 - 23465, 1997.
- Kursinski, E.R., S. Leroy, and B. Herman,** The radio occultation technique, *J. Atmos. Solar-Terr. Phys.*, 11, 53-114, 2000.
- Kursinski, E.R., S. Syndergaard, D. Flittner, D. Feng, G. Hajj, B. Herman; D. Ward and T. Yunck,** A microwave occultation observing system optimized to characterize atmospheric water, temperature and geopotential via absorption, *J. Atmos. Oceanic Technol.*, 19, 1897-1914, 2002.
- Landolt-Börnstein,** *Geophysics of the Solid Earth, the Moon and the Planets – Numerical Data and Functional Relationships in Science and Technology*, Vol. V/2a (Fuchs, K., and H. Stoffel, Eds.), 332–336, Springer Verlag, Berlin–Heidelberg, 1984.

- Leroy, S.S.**, Amplitude of an occultation signal in three dimensions, *Unpublished Script (pers. communications)*, 2001.
- Leroy, S.S., J.A. Dykema, and J.G. Anderson**, Climate benchmarking using GNSS occultation, in *Atmosphere and Climate: Studies by Occultation Methods*, U. Foelsche, G. Kirchengast, A. K. Steiner (Eds.), Springer, Berlin-Heidelberg-New York, 303-314, 2006.
- Liebe, H.J., G. Hufford, and M. Cotton**, Propagation Modeling of moist air and suspended water/ice particles at frequencies below 1000 GHz, in *52nd Specialists Meeting of the Electromagnetic Wave Propagation Panel*, p. 542, AGARD, 1993.
- Melbourne, W.G., E. Davis, C. Duncan, G. Hajj, K. Hardy, E. Kursinski, T. Meehan, L. Young, and T. Yunck**, The application of space borne GPS to atmospheric limb sounding and global change monitoring, *JPL Publ.*, 94-18, Pasadena, California, 1994.
- Nielsen, A.S., M.S. Lohmann, P. Høeg, H.-H. Benzon, A.S. Jensen, T. Kuhn, C. Mel-sheimer, S.A. Buehler, P. Eriksson, L. Gradinarsky, C. Jiménez, and G. Elgered**, Characterization of ACE+ LEO-LEO Radio Occultation Measurements, *DMI-IEP-CUT Tech. Rep. ESTEC contract no. 16743/02/NL/FF*, DMI, Copenhagen, Denmark, 2005.
- Ramsauer, J. , and G. Kirchengast**, Sensitivity of atmospheric profiles retrieved from GNSS radio occultation data to instrumental errors, *Techn. Report for ESA/ESTEC No. 6/2001*, Inst. for Geophys., Astrophys., and Meteorol., Univ. of Graz, Austria, 2001.
- Rieder, M.J., and G. Kirchengast**, Error analysis for mesospheric temperature profiling by absorptive occultation sensors, *Ann. Geophys.*, 19, 71–81, 2001a.
- Rieder, M.J., and G. Kirchengast**, Error analysis and characterization of atmospheric profiles retrieved from GNSS occultation data, *J. Geophys. Res.*, 106, 31, 755–31,770, 2001b.
- Rodgers, C.**, *Inverse Methods for atmospheric sounding – Theory and Practice*, World Scientific Publishing, Singapore, 2000.
- Salby, M.L.**, *Fundamentals of Atmospheric Physics*, Academic Press, San Diego, 1996.
- Schanda, E.**, *Physical Fundamentals of Remote Sensing*, Springer, Berlin, 1986.
- Smith, E.K., and S. Weintraub**, The constants in the equation for atmospheric refractive index at radio frequencies, *Proceedings of the I.R.E.*, 41, 1035-1037, 1953.
- Sokolovskiy, S.**, Inversion of radio occultation amplitude data, *Radio Sci.*, 35, 97-105, 2000.
- Steiner, A.K.**, High-resolution sounding of key climate variables using the radio occultation technique, *IGAM Wissenschaftl. Ber.-3/1998*, Inst. for Geophys., Astrophys., and Meteorol., Univ. of Graz, Austria, 1998.
- Steiner, A.K., G. Kirchengast, and H.P. Ladreiter**, Inversion, error analysis and validation of GPS/MET occultation data, *Ann. Geophysicae*, 17, 122-138, 1999.
- Steiner, A.K., and G. Kirchengast**, Ensemble-based analysis of errors in atmospheric profiles retrieved from GNSS occultation data, in *Occultations for Probing the Atmosphere and Climate*, G. Kirchengast, U. Foelsche, A.K. Steiner (Eds.), Springer, Berlin-Heidelberg-New York, 149-160, 2004.
- Steiner, A.K., and G. Kirchengast**, Error analysis for GNSS radio occultation data based on ensembles of profiles from end-to-end simulations, *J. Geophys. Res.*, 110, D15307, doi: 10.1029/2004JD005251, 2005.

Syndergaard, S., Modeling the impact of the Earth's oblateness on the retrieval of temperature and pressure profiles from limb sounding, *J. Atmos. Terr. Phys.*, 60, 171-180, 1998.

Syndergaard, S., Retrieval analysis and methodologies in atmospheric limb sounding using the GNSS radio occultation technique. *DMI Scient. Report 99-6*, Danish Meteorol. Institute, Copenhagen, Denmark, 1999.

Vorob'ev, V.V., and T.G. Krasnil'nikova, Estimation of the accuracy of the atmospheric refractive index recovery from doppler shift measurements at frequencies used in the NAVSTAR system, *Phys. of Atmos. and Oceans*, 29, 602-609, 1994.

– end of document –